



Unveiling galaxy pair alignment in cosmic filaments: A 3D exploration using EAGLE simulation

Suman Sarkar ^a, Biswajit Pandey ^b

^aDepartment of Physics, Indian Institute of Technology Kharagpur, West Bengal - 721302, India.

^bDepartment of Physics, Visva-Bharati University, Santiniketan, West Bengal - 731235, India.

E-mail: suman2reach@gmail.com, biswap@visva-bharati.ac.in

Abstract. We investigate how galaxy pairs are oriented in three dimensions within cosmic filaments using data from the EAGLE simulation. We identify filament spines using DisPerSE and isolate galaxies residing in filamentary environments. Employing a FoF algorithm, we delineate individual filaments and determine their axes by diagonalizing the moment of inertia tensor. The orientations of galaxy pairs relative to the axis of their host filament are analyzed. Our study covers diverse subsets of filaments identified through varying linking lengths, examining how galaxy pairs align with the filament axis across different spatial parameters such as pair separation and distance from the filament spine. We observe a nearly uniform probability distribution for the cosine of the orientation angle, which is nearly identical in each case. We also investigate the effects of redshift space distortions and confirm that the probability distributions remain uniform in both real space and redshift space. To validate our approach, we conduct Monte Carlo simulations using various theoretical probability distributions. Our analysis does not reveal any evidence of preferential alignment of galaxy pairs within cosmic filaments in hydrodynamical simulations.

Keywords: Large-scale structure of the universe: cosmic web; Galaxies: galaxy evolution - hydrodynamical simulations.

Contents

1	Introduction	1
2	Data	3
3	Methods of analysis	3
3.1	Finding galaxies in filaments using DisPerSE	3
3.2	Identification of filament groups	4
3.3	Determination of filament axis	5
3.4	Identification of galaxy pairs within filaments and analyzing their orientations	5
4	Results	5
5	Conclusions	9
A	Validating the method using controlled simulations	14

1 Introduction

Galaxies, the building blocks of the universe, are known to be distributed along a complex, interconnected network of clusters, filaments and sheets surrounded by vast empty regions. This network of galaxies is often referred to as the “cosmic web” [1]. The galaxies and their host dark matter halos residing in different cosmic web environments, experience the tidal force from the surrounding large-scale structures (LSS). Various observations suggest that the tidal force from the LSS can influence the orientation of the galaxies [2–6]. It has been reported that the major axes of the galaxies in filaments and sheets align preferentially along the filament axes and the plane of the sheet respectively [7–13]. The dark matter halos in cosmological simulations are also known to have specific alignment with respect to their host cosmic web environment [14–17].

Besides the alignment of the galaxies and their host dark matter halos, the alignment of the galaxy pairs with their host filaments has been also reported in the literature [18, 19]. The filaments are thread-like structures that connect the galaxy clusters [20, 21]. They represent the denser parts of the cosmic web and host $\sim 40\% - 45\%$ of the total mass in the universe [22, 23]. A large number of close galaxy pairs are located inside the filaments. The galaxies in pairs are interacting gravitationally with their companions as well as with their embedding large-scale environments. The preferential alignment of the galaxy pairs with the filament axes may arise due to a complex interplay of the gravitational forces operating on small and large-scales. Studying such alignment can provide important insights into the dynamics of the cosmic web. Further, both galaxy interactions [24–28] and the large-scale environments [29–38] are known to influence the galaxy properties and their evolution. Understanding the alignment may also provide crucial information on the formation and evolution of galaxies.

The galaxy pairs in observations are generally identified by applying cuts on the projected separation and the velocity difference [27, 39, 40]. It is difficult to ensure that the two members in such pairs are close in three dimension. Some of the pairs may purely arise due to chance superposition in the high-density regions [41]. Further, the galaxies are mapped in

the redshift space where the peculiar velocities distort the clustering pattern. The redshift space distortions (RSD) is a major obstacle in measuring the orientation of galaxy pairs with respect to the filaments. Previous works [18, 19] measure the projected angle between the orientations of the filament and the galaxy pairs. The filaments and the galaxy pairs are projected on the plane of the sky to minimise the affects of RSD. They find $\sim 15\% - 25\%$ excess of aligned pairs in filaments compared to a random distribution. The total number of pairs associated to filaments in these works are 3012 and 4614 respectively. The hydrodynamical simulations can provide larger dataset of paired galaxies that can be used to study such alignment. One can also quantify the effects of RSD by comparing the alignment signals in real and redshift space.

Any potential alignment signal highlights the significant influence of tidal fields from large-scale coherent structures on the spatial distribution of galaxies within these environments. Such alignment suggests a correlation between galaxy properties and their large-scale environments. When galaxy pairs align with filaments, it may indicate that their formation and evolution are influenced by tidal fields and gas flows along these structures. For example, this alignment could affect the efficiency of gas accretion in these galaxies. Recent studies by [42] analyze galaxy pairs in filaments and sheets using SDSS data and find that star formation rates in filaments are significantly higher than in sheets. These findings are further supported by [43], which uses data from EAGLE simulations. Further, galaxy pairs oriented along cosmic filaments can have important implications for weak lensing studies in cosmology. The preferred alignment may significantly impact measurements of cosmic shear and weak lensing, influencing shear alignment, introducing systematic effects, affecting mass reconstruction, and suggesting environmental dependencies in weak lensing signals. Accurate modeling and analysis are essential to disentangle these effects and properly interpret weak lensing observations in cosmology.

We aim to analyze data from the EAGLE simulations to measure the 3D orientation of galaxy pairs within filaments. We will use the DIScrete PERsistent Structures Extractor (DisPerSE) [44, 45] to identify galaxies residing in filamentary environments. Using a Friend of Friend (FoF) algorithm [46, 47], we will separate these galaxies into different filaments, resulting in a catalog of individual filaments. Axis of each filament will be determined by diagonalizing its moment of inertia tensor, with the primary axis represented by the eigenvector corresponding to the smallest eigenvalue. Galaxy pairs within each filament will be identified based on their 3D separation. Both filaments and galaxy pairs will be identified in three dimensions. The orientation angle between galaxy pairs and their host filament axes will be measured for all pairs within filaments. Any preferential alignment of galaxy pairs with respect to filament axes will be reflected in the probability distribution of the cosine of these orientation angles. The alignment could be influenced by both the separation between the two members of a pair and the distance of their center of mass from the filament spine. We will investigate how the alignment signal varies with both the separation between the two galaxies in each paired system and their distance from the filament spine. Additionally, we will map simulated galaxies in redshift space using their peculiar velocities and repeat the entire analysis to assess the effects of RSD on these measurements.

The structure of the paper is outlined as follows: Section 2 describes the data, Section 3 explains our methods, Section 4 discusses the results of our analysis, and Section 5 presents our conclusions.

2 Data

The EAGLE project [48, 49] consists of large-scale hydrodynamical simulations of the Lambda-Cold Dark Matter universe. These simulations have been crucial in gaining insights into the behavior of dark matter and galactic evolution. The project adopts the flat Λ CDM cosmology with $\Omega_\Lambda = 0.693$, $\Omega_m = 0.307$, $\Omega_b = 0.04825$, and $H_0 = 67.77 \text{ km s}^{-1} \text{ Mpc}^{-1}$ [50]. The simulations track the evolution of dark matter and baryons in comoving cubes of sizes 25, 50, and 100 Mpc using an advanced version of GADGET2 [51], starting from redshift 127 down to redshift 0. For this study, we focus on the final snapshot ($Snapshot = 28$) of the simulation at $z = 0$, covering a cubic volume of 100 comoving Mpc per side. The Cartesian coordinates of subhalos, represented by their center-of-potential, are extracted from the *Ref-L0100N1504_Subhalo* table [52]. Galaxies linked to these subhalos are identified using the *Ref-L0100N1504_Aperture* table, employing a spherical aperture of 30 kpc and requiring that their stellar mass is non-zero. To ensure that all unusual objects are discarded, only galaxies with $S_{spurious} = 0$ are considered, resulting in a total of 325358 galaxies with unique galaxy IDs. We consider only the galaxies with $\log(M_{\text{tot}}/M_\odot) \geq 8.5$, giving us a sample consisting of 310759 galaxies. For our analysis, we use a single data cube from the EAGLE simulation. We generate 100 realizations from the original data cube by randomly selecting 80% of the entire population each time without repetition. The DisPerSE and FoF algorithms identify slightly different sets of filaments in each realization, which enables us to estimate the uncertainties in our measurements. Reducing the sampling rate to lower levels lead to larger differences in the filament identification and greater uncertainties in the measurement of their orientations. Finally, we have 100 data cubes, each containing 248607 galaxies confined within a 100Mpc cube.

3 Methods of analysis

3.1 Finding galaxies in filaments using DisPerSE

To identify filament spines and nodes in the simulated galaxy distribution from EAGLE, we utilize the DIScrete PERsistent Structures Extractor (DisPerSE) [44, 45]. DisPerSE is a scale-independent topological algorithm that delineates the geometric features of the cosmic web components. It employs the discrete Morse-Smale complex, formed by intersecting ascending and descending manifolds of discrete Morse-Smale functions. The Morse function is constructed using the Delaunay Tessellation Field Extractor (DTFE) [53, 54], which transforms the discrete galaxy distribution into a smooth density field. The intersection of these manifolds reveals critical points corresponding to maxima, minima, and saddle points in the density gradient. These critical points are categorized by their indices 0, 1, 2, and 3, representing voids, walls, filaments, and nodes, respectively. The Morse field lines connect maxima and saddle points, with the points along these lines indexed as -1, indicative of filament spines. Structures exceeding a $> 5\sigma$ persistence ratio threshold are retained to avoid identifying spurious patterns. Additionally, galaxies within $d_s \leq 2 \text{ Mpc}$ from the filament spine are considered, where d_s denotes the distance from the filament spine. To exclude galaxies near nodes, a threshold of $d_n > 3 \text{ Mpc}$ is applied, where d_n is the distance from the nearest node with a critical index of 3. The choices for d_n and d_s are somewhat subjective in our analysis. We primarily choose these values based on the typical radius of galaxy clusters and cosmic filaments. Our choices are somewhat larger than the typical radius of these structures

Linking length	0.5 Mpc	1 Mpc	2 Mpc
Number of filaments including pairs	2217 \pm 19	1524 \pm 21	170 \pm 8
Number of filaments excluding pairs	883 \pm 12	920 \pm 16	115 \pm 7
Number of pairs in all filaments	189648 \pm 620	198141 \pm 630	200726 \pm 610
Number of isolated pairs in all filaments	997 \pm 21	2638 \pm 36	3348 \pm 40

Table 1. This table shows the number of filaments and number galaxy pairs hosted within the filaments for three different linking lengths. 1σ deviations around the mean are obtained from 100 realizations randomly drawn from the EAGLE data.

to ensure that we exclude all galaxies from nodes and include all possible galaxy pairs within filaments.

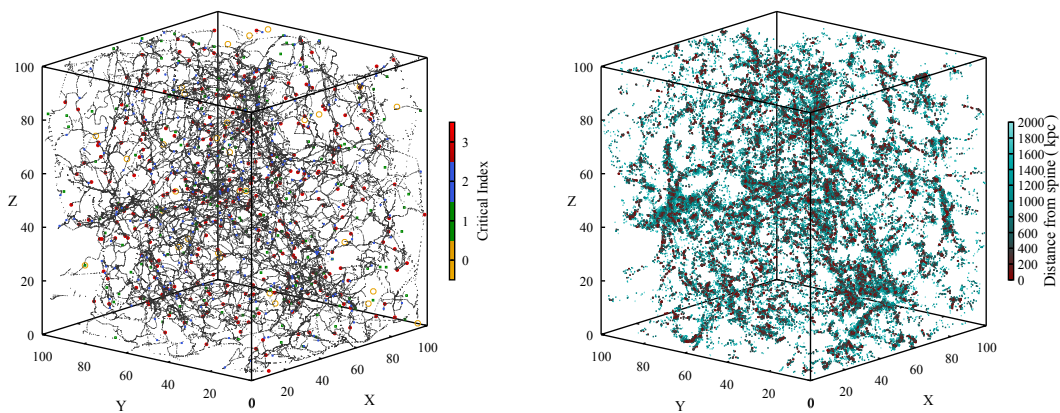


Figure 1. In the left panel of this figure, we show the critical points identified by DisPerSE in one of the 100 realizations from EAGLE. In the right panel, we display the galaxies identified in the filamentary environment for the same realization.

3.2 Identification of filament groups

First, we identify galaxies from EAGLE that reside within filamentary environments using DisPerSE. Galaxies are classified as being in a filamentary environment if they are located within 2 Mpc of the filament spine and are more than 3 Mpc away from the nearest node. Once these galaxies are identified, we group them into filament groups using the FoF algorithm [46, 47]. Each galaxy maintains a list of neighboring galaxies known as its *friends*. Groups are formed by galaxies sharing the same *friend-list*. Selecting neighboring galaxies involves a subjective decision guided by the *linking length* parameter. Typically, the linking length (l_L) is set to 0.2 times the mean inter-particle separation (\bar{r}_g). The mean inter-galactic separation of the filamentary galaxy distribution is approximately 2.5 Mpc. Initially, using $l_L = 0.2\bar{r}_g$ resulted in filament groups significantly smaller than the actual span between nodes. We carried out our analysis with different values of l_L including 0.5, 1 and 2 Mpc to ensure robustness of our results. Subsequently, for the next part of analysis, we retained only those groups containing at least 10 members. The objective here is to determine the effective direction of the filament and analyze the relative orientation of galaxy pairs within it.

3.3 Determination of filament axis

We calculate the moment of inertia tensor for a given group of galaxies identified as a filamentary system using the formula

$$\mathbf{I} = \sum_i m_i \left[\|\mathbf{r}_i\|^2 \mathbf{E}_3 - \mathbf{r}_i \otimes \mathbf{r}_i \right] \quad (3.1)$$

where m_i represents the stellar mass of the i^{th} galaxy. The position vector \mathbf{r}_i for each galaxy is determined relative to the center-of-mass (CoM) of the group, which serves as the origin. The term \mathbf{E}_3 denotes the 3×3 identity matrix, and $\mathbf{r}_i \otimes \mathbf{r}_i$ signifies the outer product of \mathbf{r}_i with itself, resulting in a matrix.

We diagonalize the moment of inertia tensor to determine its three eigenvalues λ_1 , λ_2 , and λ_3 along with corresponding eigenvectors \hat{q}_1 , \hat{q}_2 and \hat{q}_3 that define the principal axes. The three eigenvalues are obtained as roots of the characteristic equation,

$$\det[\mathbf{I} - \lambda \mathbf{E}_3] = 0. \quad (3.2)$$

The eigenvector \hat{q}_3 , corresponding to the smallest eigenvalue λ_3 , identifies the axis that defines direction of the longest extent or the smallest moment of inertia. Thus, \hat{q}_3 represents the principal direction of the filament.

3.4 Identification of galaxy pairs within filaments and analyzing their orientations

Let us begin by considering two galaxies within a filamentary group, denoted by their stellar masses m_1 and m_2 , forming a pair. We consider all galaxy pairs for which the pair separation $r_p < 200$ kpc and the mass ratio $\frac{m_1}{m_2} < 10$ where $m_1 > m_2$. It may be worthwhile to mention here that a galaxy can be part of multiple pairs. The galaxy pairs in each filament may have any possible orientation with respect to the filament axis. For each galaxy pair, we can calculate the angle between the unit vector \hat{r}_p associated with the pair separation and the unit vector \hat{q}_3 defining the axis of the host filament. The angle will be given by,

$$\theta = \cos^{-1}(\hat{r}_p \cdot \hat{q}_3) \quad (3.3)$$

We calculate the probability distribution $p(|\cos\theta|)$ utilizing the $|\cos\theta|$ values obtained for all the pairs.

Some pairs within filaments can be part of galaxy groups, where the orientation of the pairs is mainly influenced by the group environment. We are also interested in analyzing a subset of pairs that are less likely to be affected by nearby galaxies. To achieve this, we define ‘‘isolated pairs’’ as those where no other galaxies exist within a distance of 300 kpc from each member of the pair.

4 Results

In the left panel of [Figure 1](#), we display critical points identified by DisPerSE from one randomly sampled realization of the EAGLE simulation. Galaxies located within a distance $d_s \leq 1$ Mpc from the filament spine and farther than $d_n > 2$ Mpc from the nodes are identified as part of filamentary environments. These galaxies are collectively shown in the right panel of [Figure 1](#) for the same realization. To analyze individual filaments, we apply the FoF algorithm to datasets comprising galaxies within filamentary environments. The filamentary

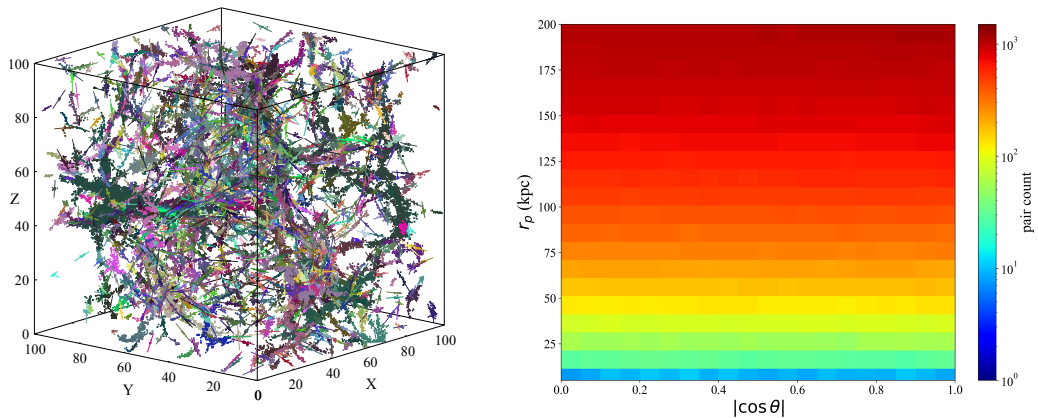


Figure 2. In the left panel of this figure, filament groups identified by FoF using a linking length of 1 Mpc are displayed, with each filament axis represented by a straight line. The right panel shows the number of pairs available for various combinations of r_p and $|\cos\theta|$ for the same linking length. Here θ is the angle between any galaxy pair and its host filament.

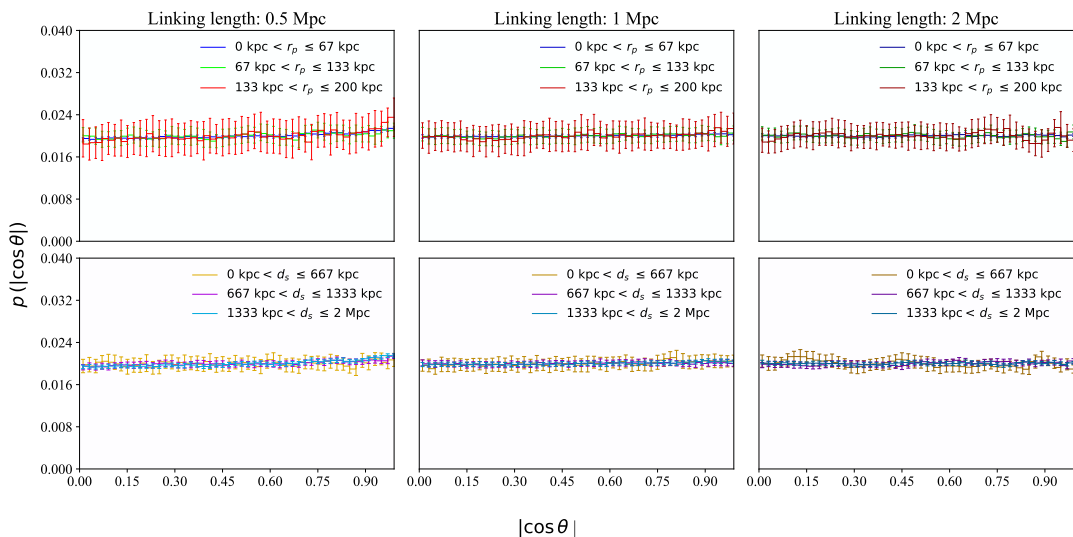


Figure 3. The different panels of this figure show the probability distribution function (PDF) of $|\cos\theta|$ for different r_p (top) and d_s (bottom) bins. The 1σ errorbars shown here are obtained from 100 random realizations drawn from the EAGLE simulation. The PDFs are shown for three different linking lengths 0.5 Mpc (left), 1 Mpc (middle) and 2 Mpc (right).

groups, identified using a linking length of 1 Mpc from the same realization of EAGLE data are shown in the left panel of [Figure 2](#). The axis of each filamentary group is represented by a straight line in this figure. We isolate galaxy pairs within each filamentary group and measure the angle between the pair separation vector and the axis of the host filament for all such pairs.

The 2D histogram in the right panel of [Figure 2](#) shows the number of available galaxy pairs in filamentary environments for different combinations of pair separation r_p and $|\cos\theta|$.

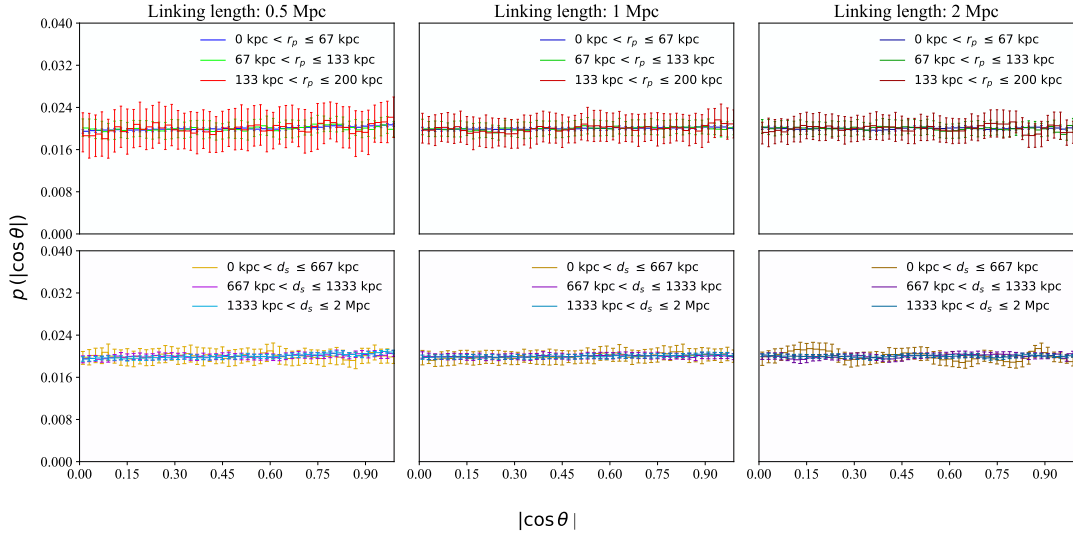


Figure 4. Same as Figure 4 but for the case where the galaxy pairs are excluded before finding the orientation of the filaments.

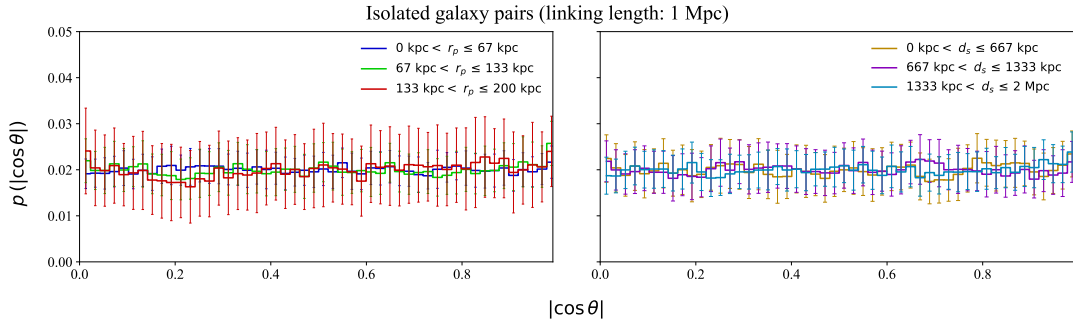


Figure 5. Different panels of this figures show the PDF of $|\cos\theta|$ in different r_p and d_s bins for the isolated pairs. The 1σ error bars shown in each case are derived from 100 random realizations drawn from the EAGLE simulation.

Here θ denotes the angle between the pair separation vector and the axis of the filament hosting the pair. The plot shows that the number of galaxy pairs at any given separation (r_p) is nearly independent of the orientation of the pairs relative to the axis of their host filaments. A gradient along the r_p axis indicates that the number of available pairs gradually increases with separation, for $r_p \leq 200$ kpc. The results in this figure do not suggest any preferential alignment of galaxy pairs within cosmic filaments.

The FoF algorithm employed to identify distinct filaments relies on a user-defined parameter known as the linking length. Varying this parameter yields different sets of identified filaments. Therefore, it is crucial to repeat the analysis using various linking lengths. To address this, we conduct our analysis using three different linking lengths: 0.5 Mpc, 1 Mpc, and 2 Mpc. The probability distributions of $|\cos\theta|$ for these linking lengths are presented in the left, middle, and right panels of Figure 3.

Any potential alignment signal for galaxy pairs is expected to depend on both the pair

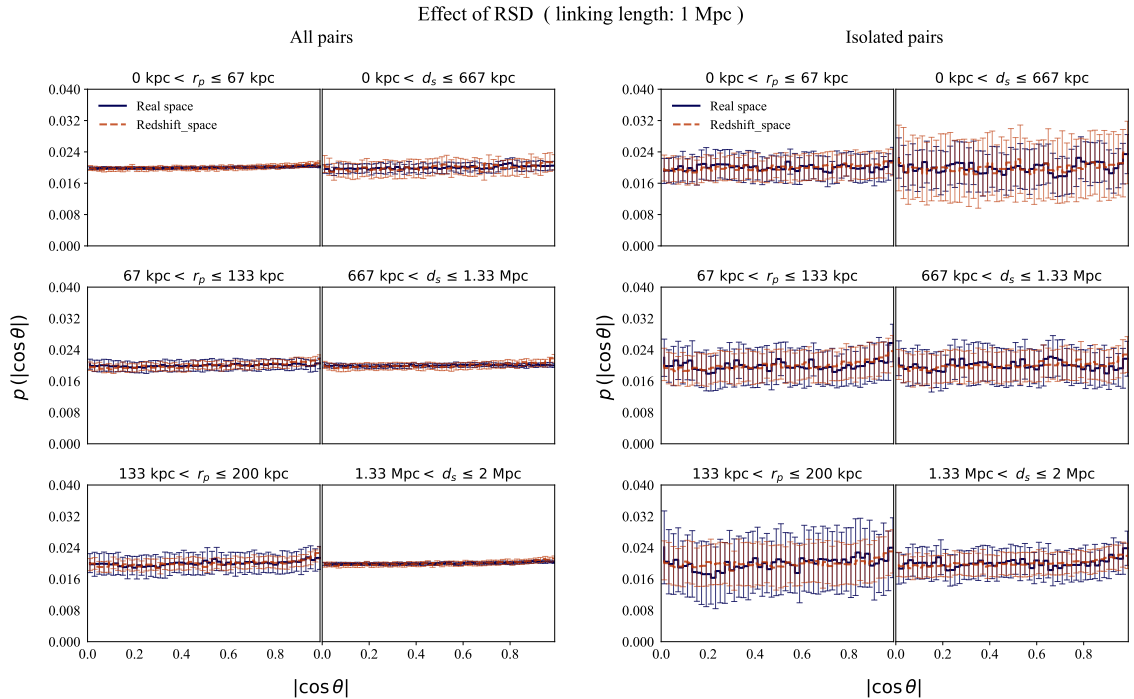


Figure 6. This figure shows the PDF of $|\cos\theta|$ estimated in real and redshift space for linking length 1 Mpc are compared for different r_p and d_s bins. 1σ error bars are drawn from 100 random realizations drawn from the EAGLE simulation. In each case, the $p(|\cos\theta|)$ for all the available pairs are shown on the left. The same is shown for the isolated pairs on right.

separation (r_p) and the distance of the pairs from the filament spine (d_s). With this in mind, we examine the orientation of galaxy pairs within filaments across different ranges of r_p and d_s .

For a linking length of 0.5 Mpc, the probability distributions of $|\cos\theta|$ for distinct intervals of r_p and d_s are respectively shown in the top and bottom left panels of Figure 3. 100 bins are used to calculate the probability distribution of $\cos\theta$ in each case and throughout the rest of our analysis. Results from the top and bottom left panels indicate a nearly uniform probability distribution for each range of r_p and d_s . This further suggests that galaxy pairs do not exhibit any preferential alignment relative to filament axes, regardless of their distance from the filament spine and for any pair separation.

Results for the other two linking lengths, 1 Mpc and 2 Mpc, are displayed in the middle and right panels of Figure 3. Interestingly, we observe nearly identical probability distributions of $|\cos\theta|$ across all three linking lengths considered in our analysis.

To measure the orientation of the filaments independently, we exclude the galaxy pairs when assessing filament orientation. Only the filaments containing at least 10 galaxies, after excluding paired galaxies, are considered. We then repeat our measurements of the galaxy pair orientations using these filament axes, and present the results in Figure 4. The observed trend is consistent with that in Figure 3. We show the number of filaments and galaxy pairs for each linking length in Table 1. The table also lists the number of available filaments with at least 10 galaxies after excluding the galaxy pairs.

The galaxy pairs may belong to groups residing within a filament, where local conditions

could influence the orientation of galaxy pairs relative to the filament spine. To investigate this, we repeat our analysis focusing on isolated galaxy pairs and present the results for a specific linking length ($l_L = 1$ Mpc) in [Figure 5](#). The same number of bins was used to compute the probability distributions of $|\cos\theta|$. Our findings again show a nearly uniform probability distribution across different ranges of r_p and d_s , as shown in the two panels of [Figure 5](#).

We conduct our analysis using EAGLE data in real space. However, observations from various redshift surveys map galaxies in redshift space, where peculiar velocities introduce distortions in the clustering pattern. It is crucial to examine the impact of these redshift space distortions (RSD) on the anticipated alignment signal. We map the positions of EAGLE galaxies in redshift space considering their peculiar velocities, and then repeat our analysis to assess the influence of RSD on our findings.

If \mathbf{v}_i and \mathbf{r}_i represent the velocity and real-space position of the i^{th} galaxy relative to an observer, then the redshifted position \mathbf{s}_i as measured by the observer can be estimated as,

$$\mathbf{s}_i = \mathbf{r}_i \left[1 + \frac{\mathbf{v}_i \cdot \mathbf{r}_i}{H_0 \|\mathbf{r}_i\|^2} \right]. \quad (4.1)$$

where H_0 is the present value of the Hubble parameter. The 100 Mpc box from EAGLE simulation represents the galaxy distribution at $z = 0$. From the EAGLE data, we generate 100 mock redshift space distributions by randomly placing the observer at one of the 8 corners each time. From these redshifted distributions, we extract the same number of galaxies as used in the real space analysis. We then follow the exact steps outlined in [Section 3](#) to analyze the orientation of galaxy pairs within filaments extracted from these redshift space distributions.

Some of the filaments detected in redshift space may result from the ‘‘Fingers of God’’ (FOG) effect. The orientation of galaxy pairs within these spurious filaments could influence the probability distributions of $|\cos\theta|$. We show the probability distributions of $|\cos\theta|$ for all pairs and isolated pairs in different panels of [Figure 6](#). For each type of pair, we compare the results in real space and redshift space across various ranges of r_p and d_s in separate panels of [Figure 6](#). Our findings clearly demonstrate that, despite the presence of FOGs, the probability distributions of the cosine of the orientation angles remain uniform in redshift space for each range of r_p and d_s . In each panel, the 1σ error bars for all pairs are comparable in real and redshift space. However, the error bars for the isolated pairs are relatively larger due to the smaller number of pairs in these samples.

5 Conclusions

We study 3D orientation of galaxy pairs within filaments using data from EAGLE simulation. We carried out our analysis for different subsets of filaments identified using 3 different linking lengths. We also consider the isolated pairs that are less impacted by their immediate neighbourhood. In each case, we study the orientations for galaxy pairs with different pair separation (r_p) and distance from filament spine (d_s). For each linking length, r_p and d_s , we recover a nearly identical probability distribution of $|\cos\theta|$ where θ is the angle between galaxy pair and axis of filament. We validate our method using controlled simulations as described in the [Appendix \(Appendix A\)](#). Our results are consistent with a random orientation of galaxy pairs within filaments.

The role of the large-scale environment in galaxy evolution remains a debated topic in the current literature. Our analysis shows that galaxy pairs do not exhibit any preferential alignment within filaments, both in real and redshift space. We observe a nearly uniform probability distribution of the cosine of the orientation angle for each range of r_p and d_s considered in our study. The size of the error bars differs between real and redshift space, primarily due to the presence of FOGs and the apparent elongation and compression of structures along the line of sight.

Studying the three-dimensional orientations of galaxy pairs relative to filament axes using observational datasets presents several challenges. Some earlier studies [18, 19] with SDSS data projected both filaments and galaxy pairs onto the plane of the sky, revealing a 15% – 25% excess of aligned pairs compared to a random distribution. In [18], filaments are identified using the Bisous model, which is based on a marked point process [55]. To avoid correlations between filament and galaxy pair orientations, they replace each galaxy pair with a single point during filament extraction. We carry out our analysis by both including and excluding galaxy pairs when evaluating the filament orientation.

[18] measure the alignment signal by projecting galaxy pairs and filaments onto the plane of the sky, where the orientation angle is constrained to the range of 0 to 90 degrees. In contrast, our analysis is performed in three dimensions (3D), where the orientation angle can vary between 0 and 180 degrees. The earlier analysis primarily focus on measuring the alignment signal using observational datasets whereas our analysis only deals with the data from hydrodynamical simulation. Extending the interpretation of the results in previous analyses to 3D is not straightforward due to the projection effects and redshift space distortions. We cannot directly compare our results with those from earlier studies due to the differences in the applied methodologies. However, it would be interesting to explore the impact of different filament identification strategies on potential alignment signals. Some caveats in our analysis are related to the identification of the filaments using DisPerSE. DisPerSE identifies structures based on their “persistence”, which reflects how long a structure persists across different smoothing scales. The choice of persistence threshold can significantly affect the resulting filament spines. Higher thresholds may lead to missing smaller or weaker filaments, while a very low threshold can result in noisy structures or false positives. The choice of smoothing scale and number of smoothing can also influence how the filaments are traced. Different choices of these parameters may lead to different sets of filaments. Further studies with different filament identifications techniques are necessary before arriving at a definite conclusion on this issue.

The primary objective of our study is to perform a 3D analysis of galaxy pair alignment within cosmic filaments using data from a hydrodynamical simulation. This represents the first 3D analysis of galaxy pair alignment in cosmic filaments, and our findings show no evidence of alignment signals in the simulations. It would be interesting to carry out a similar 3D analysis using observational data to investigate whether galaxy pair alignment signals exist in the real universe. We plan to pursue this investigation in future work.

Data availability

Data used for this study is publicly available in the database of the EAGLE project. Data generated through this project can be shared upon reasonable request to the authors.

Acknowledgement

The authors thank the anonymous reviewer for his insightful suggestions and comments. SS thanks DST-SERB for support through the NPDP project PDF/2022/000149. SS also thanks Prof. Somnath Bharadwaj for useful discussions. BP would like to acknowledge financial support from the SERB, DST, Government of India through the project CRG/2019/001110. BP would also like to acknowledge IUCAA, Pune for providing support through associateship programme. The authors acknowledge the Virgo Consortium for making their simulation data publicly available. The EAGLE simulations were performed using the DiRAC-2 facility at Durham, managed by the ICC, and the PRACE facility Curie based in France at TGCC, CEA, Bruyères-le-Châtel.

References

- [1] J.R. Bond, L. Kofman and D. Pogosyan, *How filaments of galaxies are woven into the cosmic web*, *Nature* **380** (1996) 603 [[astro-ph/9512141](#)].
- [2] D.G. Lambas, E.J. Groth and P.J.E. Peebles, *Alignments of Brightest Cluster Galaxies with Large-Scale Structures*, *AJ* **95** (1988) 996.
- [3] J. Lee and U.-L. Pen, *Detection of Galaxy Spin Alignments in the Point Source Catalog Redshift Survey Shear Field*, *ApJ Letters* **567** (2002) L111.
- [4] E. Donoso, A. O’Mill and D.G. Lambas, *Alignment between luminous red galaxies and surrounding structures at $z \sim 0.5$* , *MNRAS* **369** (2006) 479 [[astro-ph/0603471](#)].
- [5] J. Lee and P. Erdogdu, *The Alignments of the Galaxy Spins with the Real-Space Tidal Field Reconstructed from the 2MASS Redshift Survey*, *ApJ* **671** (2007) 1248 [[0706.1412](#)].
- [6] A. Hirv, J. Pelt, E. Saar, E. Tago, A. Tamm, E. Tempel et al., *Alignment of galaxies relative to their local environment in SDSS-DR8*, *A&A* **599** (2017) A31 [[1611.08378](#)].
- [7] B.J.T. Jones, R. van de Weygaert and M.A. Aragón-Calvo, *Fossil evidence for spin alignment of Sloan Digital Sky Survey galaxies in filaments*, *MNRAS* **408** (2010) 897 [[1001.4479](#)].
- [8] Y. Zhang, X. Yang, H. Wang, L. Wang, H.J. Mo and F.C. van den Bosch, *Alignments of Galaxies within Cosmic Filaments from SDSS DR7*, *ApJ* **779** (2013) 160 [[1309.3847](#)].
- [9] E. Tempel and N.I. Libeskind, *Galaxy Spin Alignment in Filaments and Sheets: Observational Evidence*, *ApJ Letters* **775** (2013) L42 [[1308.2816](#)].
- [10] E. Tempel, R.S. Stoica and E. Saar, *Evidence for spin alignment of spiral and elliptical/S0 galaxies in filaments*, *MNRAS* **428** (2013) 1827 [[1207.0068](#)].
- [11] Y. Zhang, X. Yang, H. Wang, L. Wang, W. Luo, H.J. Mo et al., *Spin Alignments of Spiral Galaxies within the Large-scale Structure from SDSS DR7*, *ApJ* **798** (2015) 17 [[1409.7150](#)].
- [12] Y.-C. Chen, S. Ho, J. Blazek, S. He, R. Mandelbaum, P. Melchior et al., *Detecting galaxy-filament alignments in the Sloan Digital Sky Survey III*, *MNRAS* **485** (2019) 2492 [[1805.00159](#)].
- [13] A. Krolewski, S. Ho, Y.-C. Chen, P.F. Chan, A. Tenneti, D. Bizyaev et al., *Alignment between Filaments and Galaxy Spins from the MaNGA Integral-field Survey*, *ApJ* **876** (2019) 52 [[1902.09797](#)].
- [14] M.A. Aragón Calvo, *Morphology and Dynamics of the Cosmic Web*, Ph.D. thesis, University of Groningen, Netherlands, Nov., 2007.
- [15] Y. Zhang, X. Yang, A. Faltenbacher, V. Springel, W. Lin and H. Wang, *The Spin and Orientation of Dark Matter Halos Within Cosmic Filaments*, *ApJ* **706** (2009) 747 [[0906.1654](#)].

- [16] N.I. Libeskind, Y. Hoffman, A. Knebe, M. Steinmetz, S. Gottlöber, O. Metuki et al., *The cosmic web and the orientation of angular momenta*, *MNRAS* **421** (2012) L137 [[1201.3365](#)].
- [17] P. Ganeshaiah Veena, M. Cautun, R. van de Weygaert, E. Tempel, B.J.T. Jones, S. Rieder et al., *The Cosmic Ballet: spin and shape alignments of haloes in the cosmic web*, *MNRAS* **481** (2018) 414 [[1805.00033](#)].
- [18] E. Tempel and A. Tamm, *Galaxy pairs align with Galactic filaments*, *A&A* **576** (2015) L5 [[1502.02043](#)].
- [19] V. Mesa, F. Duplancic, S. Alonso, M.R. Muñoz Jofré, G. Coldwell and D.G. Lambas, *The orientation of galaxy pairs with filamentary structures: dependence on morphology*, *A&A* **619** (2018) A24 [[1808.04762](#)].
- [20] J. Einasto, M. Joeveer and E. Saar, *Structure of superclusters and supercluster formation*, *MNRAS* **193** (1980) 353.
- [21] K.A. Pimbblet, *A new algorithm for the detection of intercluster galaxy filaments using galaxy orientation alignments*, *MNRAS* **358** (2005) 256 [[astro-ph/0501181](#)].
- [22] M.A. Aragón-Calvo, R. van de Weygaert and B.J.T. Jones, *Multiscale phenomenology of the cosmic web*, *MNRAS* **408** (2010) 2163 [[1007.0742](#)].
- [23] M. Haider, D. Steinhauser, M. Vogelsberger, S. Genel, V. Springel, P. Torrey et al., *Large-scale mass distribution in the Illustris simulation*, *MNRAS* **457** (2016) 3024 [[1508.01525](#)].
- [24] R.B. Larson and B.M. Tinsley, *Star formation rates in normal and peculiar galaxies.*, *ApJ* **219** (1978) 46.
- [25] E.J. Barton, M.J. Geller and S.J. Kenyon, *Tidally Triggered Star Formation in Close Pairs of Galaxies*, *ApJ* **530** (2000) 660 [[astro-ph/9909217](#)].
- [26] D.G. Lambas, P.B. Tissera, M.S. Alonso and G. Coldwell, *Galaxy pairs in the 2dF survey - I. Effects of interactions on star formation in the field*, *MNRAS* **346** (2003) 1189 [[astro-ph/0212222](#)].
- [27] M. Sol Alonso, D.G. Lambas, P. Tissera and G. Coldwell, *Effects of galaxy interactions in different environments*, *MNRAS* **367** (2006) 1029 [[astro-ph/0511362](#)].
- [28] S.L. Ellison, D.R. Patton, L. Simard, A.W. McConnachie, I.K. Baldry and J.T. Mendel, *Galaxy pairs in the Sloan Digital Sky Survey - II. The effect of environment on interactions*, *MNRAS* **407** (2010) 1514 [[1002.4418](#)].
- [29] B. Pandey and S. Bharadwaj, *The luminosity, colour and morphology dependence of galaxy filaments in the Sloan Digital Sky Survey Data Release Four*, *MNRAS* **372** (2006) 827 [[astro-ph/0601179](#)].
- [30] B. Pandey and S. Bharadwaj, *The luminosity-bias relation from filaments in the Sloan Digital Sky Survey Data Release Four*, *MNRAS* **377** (2007) L15 [[astro-ph/0701615](#)].
- [31] J.M. Scudder, S.L. Ellison and J.T. Mendel, *The dependence of galaxy group star formation rates and metallicities on large-scale environment*, *MNRAS* **423** (2012) 2690 [[1204.2828](#)].
- [32] H.E. Luparello, M. Lares, D. Paz, C.Y. Yaryura, D.G. Lambas and N. Padilla, *Brightest group galaxies and the large-scale environment*, *MNRAS* **448** (2015) 1483 [[1502.01221](#)].
- [33] B. Pandey and S. Sarkar, *How much a galaxy knows about its large-scale environment?: An information theoretic perspective*, *MNRAS* **467** (2017) L6 [[1611.00283](#)].
- [34] J. Lee, *A New Perspective on the Large-scale Tidal Effect on the Galaxy Luminosity and Morphology*, *ApJ* **867** (2018) 36 [[1805.07492](#)].
- [35] M. Einasto, M. Gramann, C. Park, J. Kim, B. Deshev, E. Tempel et al., *Supercluster A2142 and collapse in action: infalling and merging groups and galaxy transformations*, *A&A* **620** (2018) A149 [[1810.12122](#)].

- [36] B. Pandey and S. Sarkar, *Exploring galaxy colour in different environments of the cosmic web with SDSS*, *MNRAS* **498** (2020) 6069 [2002.08400].
- [37] S. Sarkar and B. Pandey, *A study on the statistical significance of mutual information between morphology of a galaxy and its large-scale environment*, *MNRAS* **497** (2020) 4077 [2003.13974].
- [38] S. Sarkar, B. Pandey and A. Das, *On the origin of red spirals: does assembly bias play a role?*, *JCAP* **2022** (2022) 024 [2111.11252].
- [39] S.L. Ellison, D.R. Patton, L. Simard and A.W. McConnachie, *Galaxy Pairs in the Sloan Digital Sky Survey. I. Star Formation, Active Galactic Nucleus Fraction, and the Mass-Metallicity Relation*, *AJ* **135** (2008) 1877 [0803.0161].
- [40] A. Das, B. Pandey and S. Sarkar, *Do Minor Interactions Trigger Star Formation in Galaxy Pairs?*, *Research in Astronomy and Astrophysics* **23** (2023) 095026 [2207.03968].
- [41] M.S. Alonso, P.B. Tissera, G. Coldwell and D.G. Lambas, *Galaxy pairs in the 2dF survey - II. Effects of interactions on star formation in groups and clusters*, *MNRAS* **352** (2004) 1081 [astro-ph/0401455].
- [42] A. Das, B. Pandey and S. Sarkar, *Galaxy Interactions in Filaments and Sheets: Effects of the Large-scale Structures Versus the Local Density*, *Research in Astronomy and Astrophysics* **23** (2023) 025016 [2209.14194].
- [43] A. Das, B. Pandey and S. Sarkar, *Galaxy Interactions in Filaments and Sheets: Insights from EAGLE Simulations*, *Research in Astronomy and Astrophysics* **23** (2023) 115018 [2303.16826].
- [44] T. Sousbie, C. Pichon and H. Kawahara, *The persistent cosmic web and its filamentary structure - II. Illustrations*, *MNRAS* **414** (2011) 384 [1009.4014].
- [45] T. Sousbie, *The persistent cosmic web and its filamentary structure - I. Theory and implementation*, *MNRAS* **414** (2011) 350 [1009.4015].
- [46] J.P. Huchra and M.J. Geller, *Groups of Galaxies. I. Nearby groups*, *ApJ* **257** (1982) 423.
- [47] A.A. Berlind, J. Frieman, D.H. Weinberg, M.R. Blanton, M.S. Warren, K. Abazajian et al., *Percolation Galaxy Groups and Clusters in the SDSS Redshift Survey: Identification, Catalogs, and the Multiplicity Function*, *ApJS* **167** (2006) 1 [astro-ph/0601346].
- [48] J. Schaye, R.A. Crain, R.G. Bower, M. Furlong, M. Schaller, T. Theuns et al., *The EAGLE project: simulating the evolution and assembly of galaxies and their environments*, *MNRAS* **446** (2015) 521 [1407.7040].
- [49] R.A. Crain, J. Schaye, R.G. Bower, M. Furlong, M. Schaller, T. Theuns et al., *The EAGLE simulations of galaxy formation: calibration of subgrid physics and model variations*, *MNRAS* **450** (2015) 1937 [1501.01311].
- [50] PLANCK collaboration, *Planck 2013 results. I. Overview of products and scientific results*, *Astron. Astrophys.* **571** (2014) A1 [1303.5062].
- [51] V. Springel, *The cosmological simulation code GADGET-2*, *MNRAS* **364** (2005) 1105 [astro-ph/0505010].
- [52] S. McAlpine, J.C. Helly, M. Schaller, J.W. Trayford, Y. Qu, M. Furlong et al., *The EAGLE simulations of galaxy formation: Public release of halo and galaxy catalogues*, *Astronomy and Computing* **15** (2016) 72 [1510.01320].
- [53] W.E. Schaap and R. van de Weygaert, *Continuous fields and discrete samples: reconstruction through Delaunay tessellations*, *A&A* **363** (2000) L29 [astro-ph/0011007].
- [54] R. van de Weygaert and W. Schaap, *The Cosmic Web: Geometric Analysis*, in *Data Analysis in Cosmology*, V.J. Martínez, E. Saar, E. Martínez-González and M.J. Pons-Bordería, eds., vol. 665, pp. 291–413 (2009), DOI.

- [55] E. Tempel, R.S. Stoica, V.J. Martínez, L.J. Liivamägi, G. Castellan and E. Saar, *Detecting filamentary pattern in the cosmic web: a catalogue of filaments for the SDSS*, *MNRAS* **438** (2014) 3465 [1308.2533].

A Validating the method using controlled simulations

In this section, we assess the reliability of our method by conducting tests with controlled simulations. We create multiple controlled simulations of galaxy pairs within mock filaments using Monte Carlo simulations. We randomly generate the axis of each filament, and then position the galaxy pairs around the filament axis. The galaxy pairs are assigned orientation angles according to a specific probability distribution of $\cos\theta$, where θ represents the orientation angle. We examine three distinct types of probability distributions which are discussed below.

- **Controlled mock 1:** We simulate pairs with random orientation relative to the filament axis using a discrete probability distribution $p(\cos\theta) = \frac{1}{N_b}$, where N_b represents the number of bins used for binning $\cos\theta$. When orientations are random, the probability of any specific orientation of galaxy pairs relative to the filament axis follows a uniform distribution given by $p(\mu) = \frac{1}{(\mu_{max}-\mu_{min})}$ where $\mu = \cos\theta$ and $\mu_{min} = -1$ and $\mu_{max} = 1$ are the minimum and maximum values of μ . The discrete version of this distribution is derived by multiplying the continuous probability distribution by the bin width $\Delta\mu = \frac{\mu_{max}-\mu_{min}}{N_b}$. Hence, the discrete probability distribution for Controlled mock 1 is expressed as,

$$p(\cos\theta) = \frac{1}{N_b}$$

- **Controlled mock 2:** The probability distribution for pairs with preferential orientation perpendicular to the filament axis can be generated using the distribution $p(\cos\theta) = \frac{4}{\pi N_b} \sqrt{1 - \cos^2\theta}$. The distribution can be derived as follows. In the left panel of Figure 7, we illustrate the total probability for Controlled mock 2, represented by the shaded area which, by definition, must be equal unity. Here, we denote $\cos\theta$ as μ . If $p(\mu)$ has its maximum value α and μ spans from $\mu_{min} = -\beta$ to $\mu_{max} = \beta$, the area of the shaded region would be $\frac{1}{2}\pi\alpha\beta$. So we have $\alpha = \frac{2}{\pi}$ as $\beta = 1$. The equation of this ellipse becomes

$$\frac{\mu^2}{\beta^2} + \frac{p(\mu)^2}{\alpha^2} = 1 \tag{A.1}$$

The probability distribution of μ i.e. $\cos\theta$ can be written as

$$p(\cos\theta) = \frac{2}{\pi} \sqrt{1 - \cos^2\theta}$$

Thus, the discrete version of the probability distribution for Controlled mock 2 is given by

$$p(\cos\theta) = \frac{4}{\pi N_b} \sqrt{1 - \cos^2\theta}$$

Box size	100 Mpc
Filament length	30 Mpc
Number of pairs	5000
Maximum pair separation	200 kpc
Max distance from filament spine	2 Mpc

Table 2. This table shows the parameters used in the controlled simulations of the mock filaments and galaxy pairs in these tests.

- **Controlled mock 3:** The pairs exhibiting preferential alignment along the filament axis are governed by the distribution $p(\cos\theta) = \frac{4}{(4-\pi)N_b} \left[1 - \sqrt{1 - \cos^2\theta} \right]$. In the right panel of Figure 7, we present the probability distribution for Controlled mock 3. By definition, the shaded area in this figure must equate to unity, leading to the relationship $2\alpha\beta - \frac{1}{2}\pi\alpha\beta = 1$, where $\alpha = \frac{2}{4-\pi}$ denotes the maximum probability for parallel orientation. The equation of the ellipse describing this scenario is given by

$$\frac{\mu^2}{\beta^2} + \frac{[\alpha - p(\mu)]^2}{\alpha^2} = 1 \quad (\text{A.2})$$

Therefore, considering N_b discrete bins, the discrete version of the probability distribution is expressed as

$$p(\cos\theta) = \frac{4}{(4-\pi)N_b} \left[1 - \sqrt{1 - \cos^2\theta} \right]$$

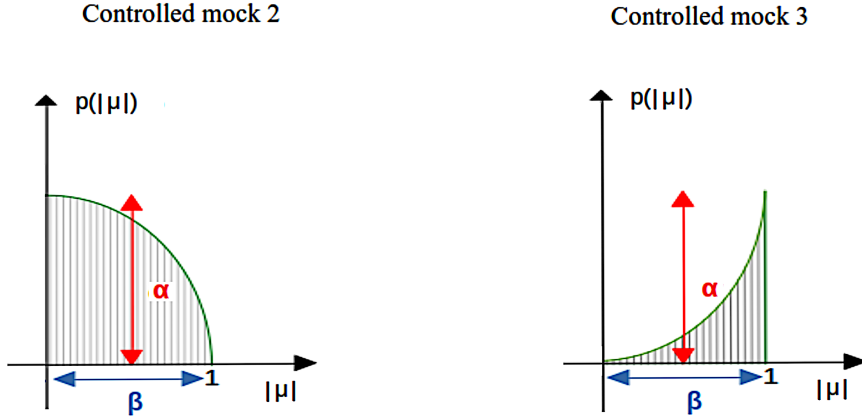


Figure 7. Schematic diagram showing the probability distributions of Controlled mock 2 and 3

We use $N_b = 100$ throughout this analysis. We ensure $\sum_{i=1}^{N_b} p(|\cos\theta_i|) = 1$, for each of the three cases, where θ_i represents the orientation angle at the center of the i^{th} bin. We generate 100 mock samples in each case to estimate the 1σ errorbars.

We attempt to reconstruct the probability distribution of galaxy pairs in these three types of mock samples using the methodologies described in Section 3. For each mock sample,

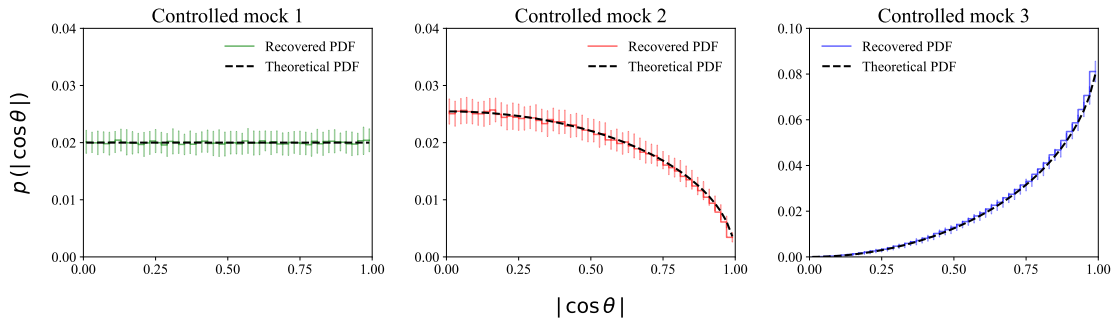


Figure 8. This figure shows the recovered and the theoretical probability distributions for the three different types of controlled mock samples. The 1σ errorbars in each case are estimated using 100 Monte-Carlo realizations. The theoretical probability distribution of $p(\cos\theta)$ in each case is multiplied by 2 since we present the probability distributions of $p(|\cos\theta|)$ in these plots.

we treat the points associated with the entire set of pairs from a single filament. Using the technique outlined in Section 3.4, we determine the Center of Mass (CoM) and the axis of the filament. Subsequently, we calculate the angle of each pair relative to the identified filament axis.

The reconstructed probability distributions of the orientation of galaxy pairs, along with their corresponding theoretical distributions, are displayed in separate panels of Figure 8. We also conducted repeated tests where we varied the parameters of the simulated filaments listed in Table 2. In every instance, we consistently recovered the theoretical probability distributions.

We observe that our method reliably recovers the theoretical probability distribution in each scenario. We also repeat our analysis by varying the length, diameter, and orientation of the simulated filaments, and find that our results are independent of these factors. However, it is worth mentioning that the simulated filaments are straight with a cylindrical geometry. They have finite length and diameter as listed in Table 2. These filaments do not have the same complex or curved geometry as those identified in the EAGLE simulation, nor are they identified using DisPerSE. As a result, filament identification mismatches are not included in this analysis.